Journal of Applied Sciences

ISSN 1812-5654

science alert

ANSInet
an open access publisher
http://ansinet.com

Journal of Applied Sciences 15 (10): 1196-1209, 2015
ISSN 1812-5654

RESEARCH ARTICLE OPEN ACCESS

DOI: 10.3923/jas.2015.1196.1209

Design and Optimization of a Tubular Permanent Magnet Linear Motor Using Finite Element Method and Permeance Analysis Method for Spray Application

[1]A.K.M. Parvez Iqbal, [2]Ishak Aris and [2]M. Norhisam
[1]Center for Advanced Mechatronics and Robotics, Universiti Tenaga Nasional, 43000, Kajang, Selangor, Malaysia
[2]Department of Electrical and Electronics Engineering, Universiti Putra Malaysia, UPM, 43400, Selangor, Malaysia

ARTICLE INFO
Article History:
Received: June 19, 2015
Accepted: October 07, 2015

Corresponding Author:
A.K.M. Parvez Iqbal
Center for Advanced Mechatronics and Robotics, Universiti Tenaga Nasional, 43000, Kajang, Selangor, Malaysia
Tel : 603-89287232

ABSTRACT
In order to overcome difficulties of using pneumatic system operated automatic spray gun, a tubular permanent magnet linear motor has been designed and developed to trigger the spray gun. Finite Element Method (FEM) is implemented in motor designing process to obtain the proper size of back yoke, coil and permanent magnet, type of materials of back yoke and PM, pitch length and the required thrust of the linear motor. Magnetic flux distribution can also be predicted from FEM analysis. Then several permeance thrust models are developed to optimize the size of the motor by analyzing the effect of thrust constant, electrical and mechanical time constant. Finally based on the optimized data the linear motor has been fabricated and tested with newly developed spray gun. During the performance test it is seen that the developed linear motor can be successfully implemented to trigger the spray gun.

Key words: Linear motor, thrust model, thrust constant, electrical time constant, mechanical time constant

INTRODUCTION

Linear motors are electro-mechanical devices that can produce linear motion directly without the use of any mechanical transmission to convert rotary motion into linear motion. Due to this mechanical simplicity the electromagnetic force can be directly applied to the payload that significantly reduces the non-linearities and disturbance caused by the backlash and additional frictional force. The linear motors provide the better dynamic performance and higher reliability over conventional rotary to linear counterparts because of the absence of mechanical gears and transmission system (Chen *et al*., 2008). Among the various linear machine topologies, tubular permanent magnet machines provide the highest efficiency and offer a high power/force density and excellent servo characteristics (Eastham, 1990). Hence, linear permanent magnet machine are being used increasingly in application as varied as manufacturing automation, electrical power generation, transportation, healthcare and house hold appliances (Masada, 1995; White *et al*., 1996; Cawthorne *et al*., 1999; Watada *et al*., 1993; Clark *et al*., 1995; Park *et al*., 2001; Utsuno *et al*., 2001). Linear motors are also useful in the semiconductor fabrication and inspection processes (Low *et al*., 1998).

The combination of cogging force and the end effect produce a large detent force for positioning the linear synchronous motor precisely. In order to reduce the detent force, field oriented control algorithm has been employed by analyzing the characteristics of thrust and normal force of the linear synchronous motor (Zhu *et al*., 2011). Beside that a high performance Nd2Fe14B/Ta thin film permanent magnet that has a high remnant flux density, high coercive force and high heat tolerance is used to develop a moving magnet type MEMS linear motor. The objectives of this study are to realize feedback positioning of the MEMS linear motor and to investigate the dynamics of the motor system

(Fujiwara *et al*., 2013). By using the repulsive magnetic forces, miniature moving-magnet type linear actuator has been developed. The 2 structures with moving magnets and other 2 with fixed magnets are studied and chosen the moving magnet types that are cheap and simple. Numerical study shows that 1 of the moving magnet structures has been achieved the objective of this study (Olaru *et al*., 2012). A hydraulic mount for passive vibration damping and a Linear Oscillatory Actuator (LOA) for active vibration damping are studied to reduce frame vibration and noise of engine mount. The result shows the active control engine mounts with LOA is more effective than the hydraulic system (Kitayama *et al*., 2012). Beside that the magnetic force generated by the linear actuator can be increased through the optimization and design of the devices air-gap magnetic field distribution. A periodic ladder structure is used for this study to manipulate the magnetic field (Lee *et al*., 2012). Meanwhile, a methodology has been developed to simulate and verify the experimental results of the axial force exerted by an electromagnet on a concentric permanent magnet (Al-Sharif *et al*., 2010). On the other hand, by using the latching theory of permanent magnet, an electromagnetic linear actuator (EMLA) has been developed to inject fuel into engine. Eddy current, dimensions of components and fringing effects are taken into account to establish the model of EMLA (Shi and Chang, 2013). Usually large amount of normal force are exerted by the single-sided linear motor during operation. A new H-module linear actuator has been developed to reduce the exerted normal force. This new system can eliminate the air suspension system that would use previously to reduce the exerted normal force (Liu *et al*., 2012).

In automatic spray operation, pneumatic system is applied to trigger the spray gun. But the main disadvantage of the pneumatic system is to control the positioning of the needle or ball valve according to the desired spray operation. Highly skilled operator as well as positioning knob is implemented to solve this problem which is time consuming and costly (Aris *et al*., 2006; Parvez Iqbal *et al*., 2011a). Addressing this issue a tubular permanent magnet linear motor has been designed and developed to trigger the spray gun. Finite Element Method (FEM) is implemented in motor design process to obtain the proper size of back yoke, coil and permanent magnet, type of materials of back yoke and PM, pitch length and the required thrust of the linear motor. Magnetic flux distribution can also be predicted from FEM analysis. Then several permeance thrust models are developed to optimize the size of the motor by analyzing the effect of thrust constant, electrical and mechanical time constant (Parvez Iqbal *et al*., 2011b; Wang and Howe, 2004; Hirata *et al*., 1992; Mizuno *et al*., 2000). Finally, based on the optimized data the linear motor has been fabricated and tested with newly developed spray gun. During the performance test it is seen that the developed linear motor can be successfully implemented to trigger the spray gun.

MATERIALS AND METHODS

The main objective of the FEM analysis is to predict the size of a linear motor that can produce a sufficient amount of thrust to trigger the spray gun. From the spring testing result, it can be decided that around 60 N thrust produced by the motor is enough to trigger the spray gun, because a link mechanism is used to trigger the spray gun. The upper part of the triggering lever was hinged with the gun body and lower part was pinned with a link. The link was directly attached to the shaft of the linear motor. A 10 mm displacement of the needle or ball valve is sufficient to fully open the nozzle of the spray unit. The triggering lever and link mechanism were designed in such a way that if the link as well as the shaft of the linear motor was moved 24 mm, the triggering lever can displace the needle or ball valve 10 mm. Therefore, during the development of the FEM model, 2 major factors were considered. One was the displacement, which was 24 mm and another was the produced thrust which was around 60 N. In order to obtain the desired results, several models have been developed by changing the number of coils and PMs as well as the size of the back yoke and the shaft. Figure 1 shows internal system of the linear motor operated spray gun.

Generating thrust model using Finite Element Method (FEM): By using the finite element method, the magnetic flux flow path, the magnetic flux density in the motor structure, which produces thrust or torque as well as the size of the linear motor can be predicted. Figure 2 shows the flow chart of the FEM analysis.

Structure modeling: For the FEM analysis, the first step was to develop the model of the proposed structure. For this research, SolidWorks software was used to develop the structure of the proposed model. All components of the model such as back yoke, coils, PM, shaft and cover plates as shown in Fig. 3 have been developed as individual parts. Then all parts were assembled to create the model of the linear motor. Figure 3 also shows the modeling environment of SolidWorks. The back yoke was designed to hold the internal part of the motor such as coil and coil casing, permanent magnets and shaft. The 2 ends of the back yoke provide the flexibility to hold the cover plates. The shaft was designed in such a way that it can hold the permanent magnet in the proper position. The 2 ends of the shaft are used to attach the linear bush and the slotted parts are used to hold the permanent magnets. The 4 coils were used in this system. The coil casing was designed in such a way that it can hold the coils and provide the minimum gap between the coils and the permanent magnets. In this design 2 mm gaps are provided between the coils. The coil wire can be shifted from 1 coil to another through the slotted part of the coil. The cover plate was designed in such a way that it can hold the linear bush and can be attached to the back yoke. Non-magnetic material was used for the cover

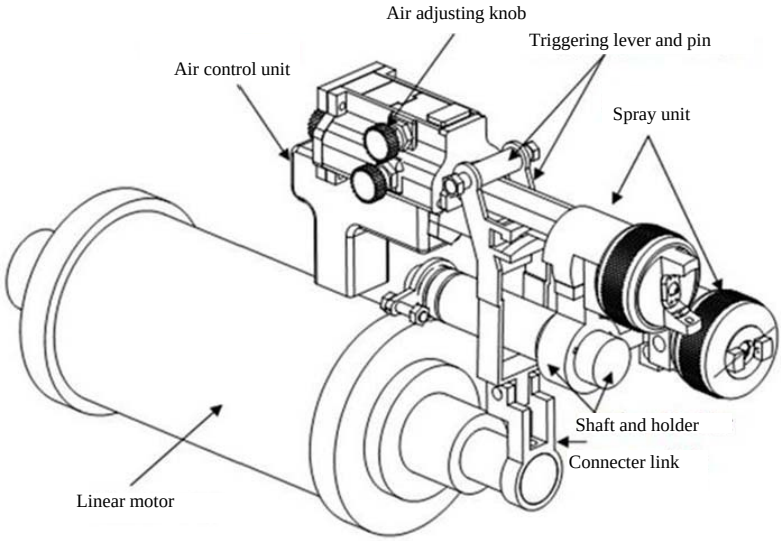

Fig. 1: Internal system of the linear motor operated spray gun

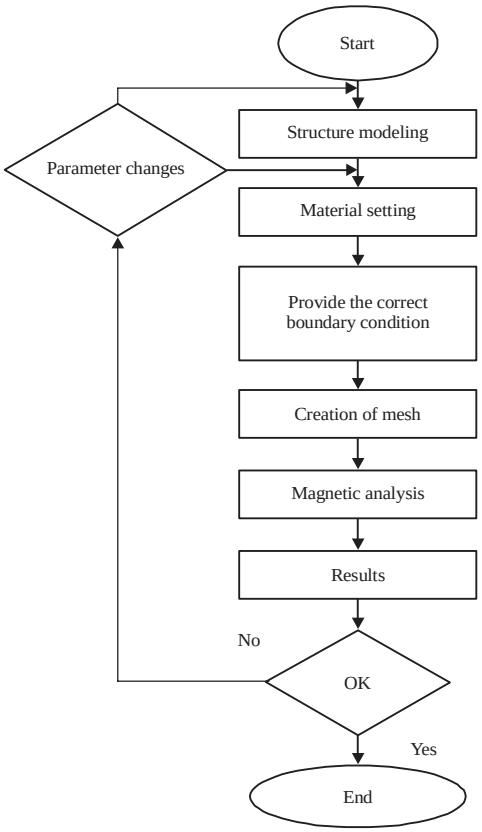

Fig. 2: Flow chart of the finite element method analysis

plate to restrict the flux flow outside the motor in a longitudinal direction. A non-magnetic material linear bush was designed in such a way that it can hold the displacement shaft in proper alignment.

Static simulation: The most important parts that were considered in the design of the linear motor were the stator and the mover. The stator was configured with the back yoke, coils and cover plates. Meanwhile the mover part consists of permanent magnets and a shaft. All of the parts were analyzed to determine the magnetic circuit behaviors and characteristics. An enclosure around the model was created to set the boundary conditions which represents the air. Then, the material and the property for each material were defined for the simulation. Figure 4a-d show the thrust model, the ANSYS modeling environment, magnetic flux distribution and the produced thrust of the linear motor. After defining the materials, the PM polarization was set. Meanwhile the coils needed to be defined according to the number of turns, injected current and input voltage. Since the analysis was magneto-static, the voltage was not considered for this simulation. Finally, the meshing process was applied to the appropriate parts to complete the simulation. After carrying out the analysis, several results were obtained. For this research, the magnetic flux density, magnetic flux flow path and directional force were considered. All of the results are shown in different color and spectrums. Each color spectrum represents the different intensity. For example, the red color for the magnetic flux density has the highest value. The area of the model focuses the red color which means that particular area will be saturated first and this situation needs to be avoided. On the other hand, the blue color represents the lower flux density. Normally the blue region occurs in the air.

Generating thrust model using Permeance Analysis Method (PAM): Figure 5 shows the flowchart of PAM method.

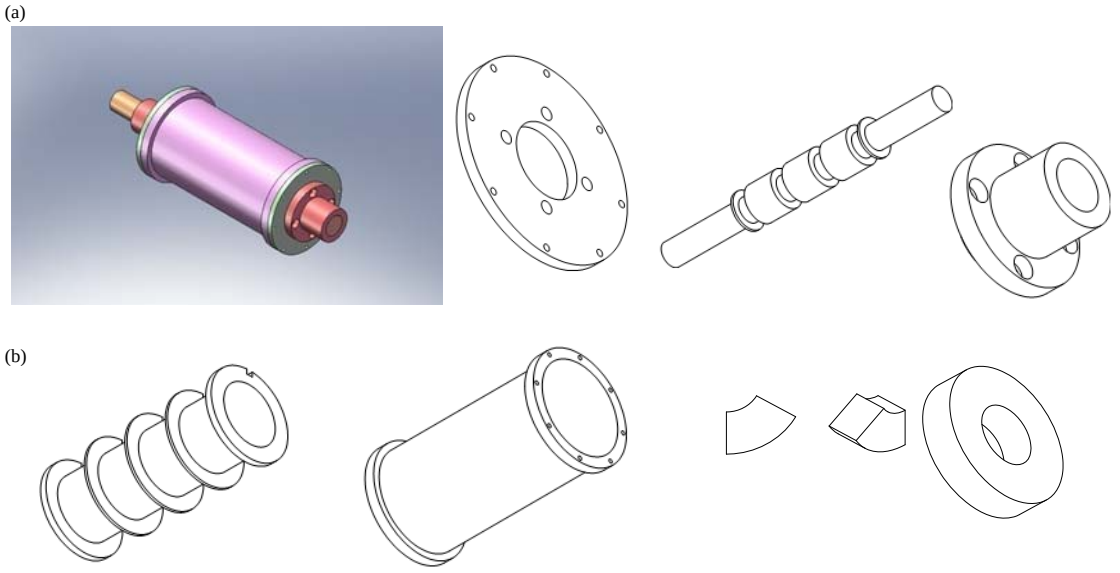

Fig. 3(a-b): Structural model of the linear motor (a) Model of the linear motor cover plate shaft linear bush and (b) Coil casing back yoke permanent magnet

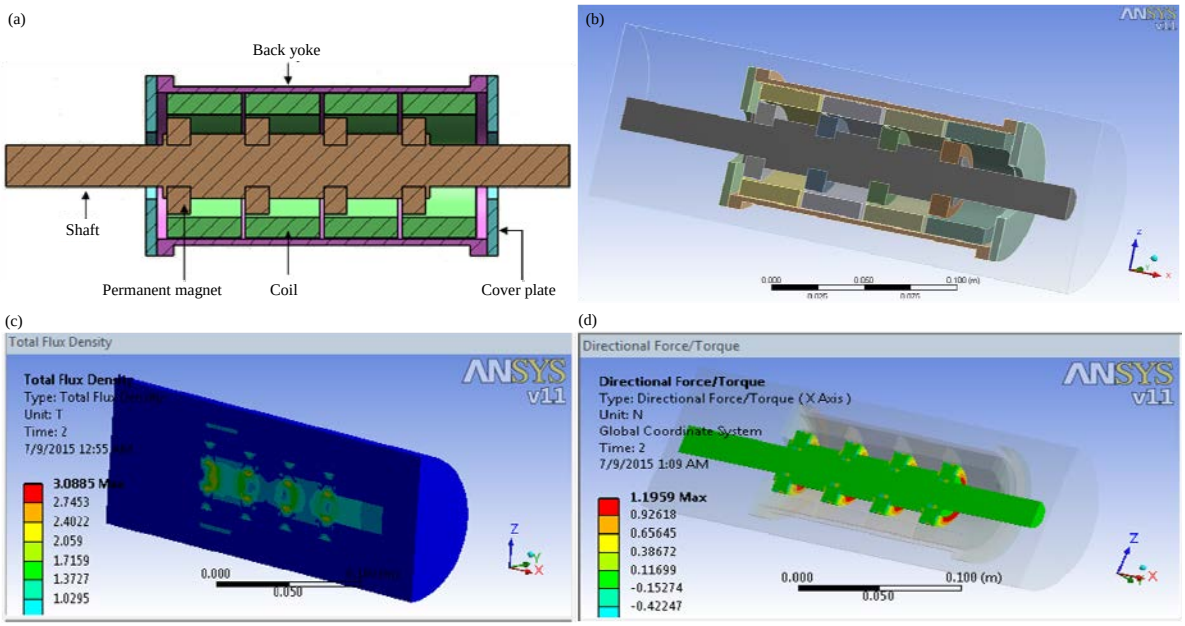

Fig. 4(a-d): Thrust model and simulation process of the linear motor, (a) Linear motor thrust model for simulation, (b) Finite element method simulation environment linear motor thrust model, (c) Magnetic flux distribution in the linear motor at finite element method simulation and (d) Thrust produced in the linear motor at finite element method simulation

Selection of permeance model and magnetic equivalent circuit: The 3 permeance models have been developed for the PAM analysis. Among these 3 models, only 1 model was selected as a PAM model for this research because it can produce an amount of thrust almost similar to the thrust in the FEM model. The total permeance value of each model was used to evaluate the magnetic flux density and thrust. For this research the thrust was calculated at the mid position of the total displacement. Because only at this position the maximum thrust can be obtained. Basically the permeance model was developed by plotting the predicted magnetic flux path at the air gap. Only 2 of the coils, namely the end coil and the middle coil of the linear motor were considered since the others are symmetrical. Figure 6 shows the selected permeance model and its equivalent magnetic circuit.

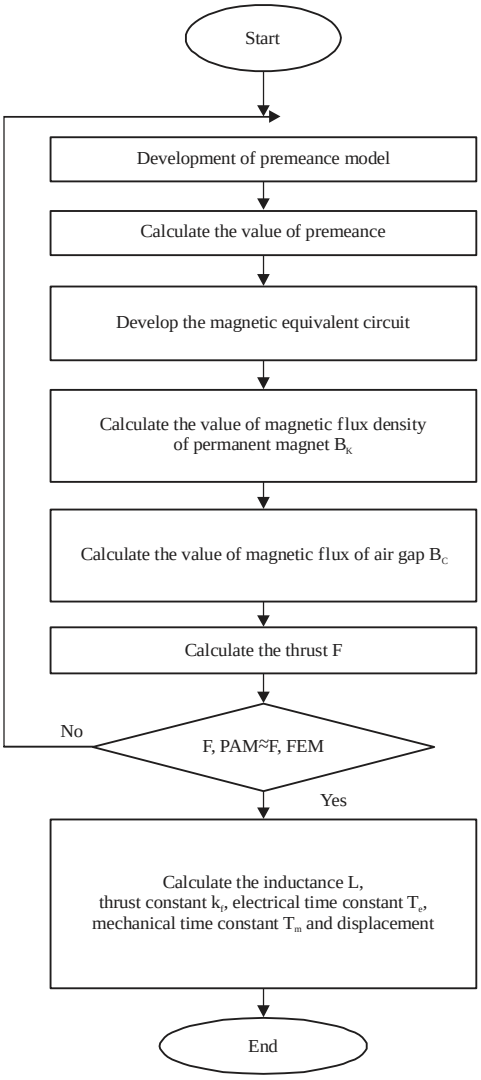

Fig. 5: Flow chart of the permeance analysis method model

As shown in Fig. 6, r_3 is the inner radius of back yoke, g is the gap between PM and coil, r_2 is the outer radius of the PM, r_1 is the inner radius of the PM, r_4 is the extended radius of the mover, w_m is the width of the PM, h_c is the height of the coil and w_c is the width of the coil. The permeances such as P_1, P2, P_3, P_4 and P_5, P_{end} and P_{middle} are expressed by the following Eq. 1-7:

$$P_1 = \mu_0 \frac{w_m}{\pi} \ln\left(\frac{r_3}{r_2}\right) \quad (1)$$

$$P_2 = 0.52\mu_0 (2\pi r_3) \quad (2)$$

$$P_3 = \mu_0 \frac{2(2\pi r_3)}{\pi} \ln\left(1+\frac{c}{h_c+g}\right) \quad (3)$$

$$P_4 = 0.52\mu_0 (2\pi r_4) \quad (4)$$

$$P_5 = \mu_0 \frac{L_m}{\pi} \ln\left(1+\frac{r_2+g-r_4}{r_4}\right) \quad (5)$$

$$P_{end} = P_1+P_2+P_3 \quad (6)$$

$$P_{middle} = \frac{(P_1+P_2+P_4)^2 + 2P_5(P_1+P_2+P_4)}{2(P_1+P_2+P_4)} \quad (7)$$

Magnetic flux density of linear motor: The permeance evaluated from the permeance models A, B and C were used to determine the operating point of Permanent Magnet (PM) B_k. Based on the hysteresis loop, the operating point for PM is determined by solving the intersection of 2 straight lines which are the B-H curve of PM and the permeance line of the motor. The slope of the permeance line depends on the angle α and can be expressed as:

$$\tan\alpha = \frac{P_T H_C h_m}{2B_r A_m}$$

where, the calculation of tan α depends on the physical properties of the permanent magnet material and the motor structure (Gieras and Wing, 2002; Zare *et al*., 2011). The physical properties of Neodymium magnets (Nd-Fe-B) were used for this calculation. Besides, P_T is the total permeance which was calculated by using Eq. 6 and 7 for end and middle position, H_c is coercive force, h_m is the height of the PM, B_r is a remanent flux density and A_m is the area of the PM used for producing flux (for this case $A_m = 2\pi r W_m$ where, r is the mean radius of PM and W_m is the width of PM). Meanwhile the PM field intensity H_k can be expressed in Eq. 8 as:

$$H_k = \frac{-B_r}{\frac{B_r}{H_c} + \tan\alpha} \quad (8)$$

where, H_k is the magnetic field intensity of the PM at the operating point. The values of B_r and H_c depend on the type of PM material used. The magnetic flux density of the PM at the operating point can be expressed in Eq. 9 as:

$$B_k = (-tak\ \alpha)H_k \quad (9)$$

where, B_k is the magnetic flux density. Using the value of B_k, the magnetic flux Φ_m at PM can be evaluated. The magnetic flux is the product of the magnetic field density at the operating point and the area of the magnet. Therefore it can be expressed in Eq. 10 as:

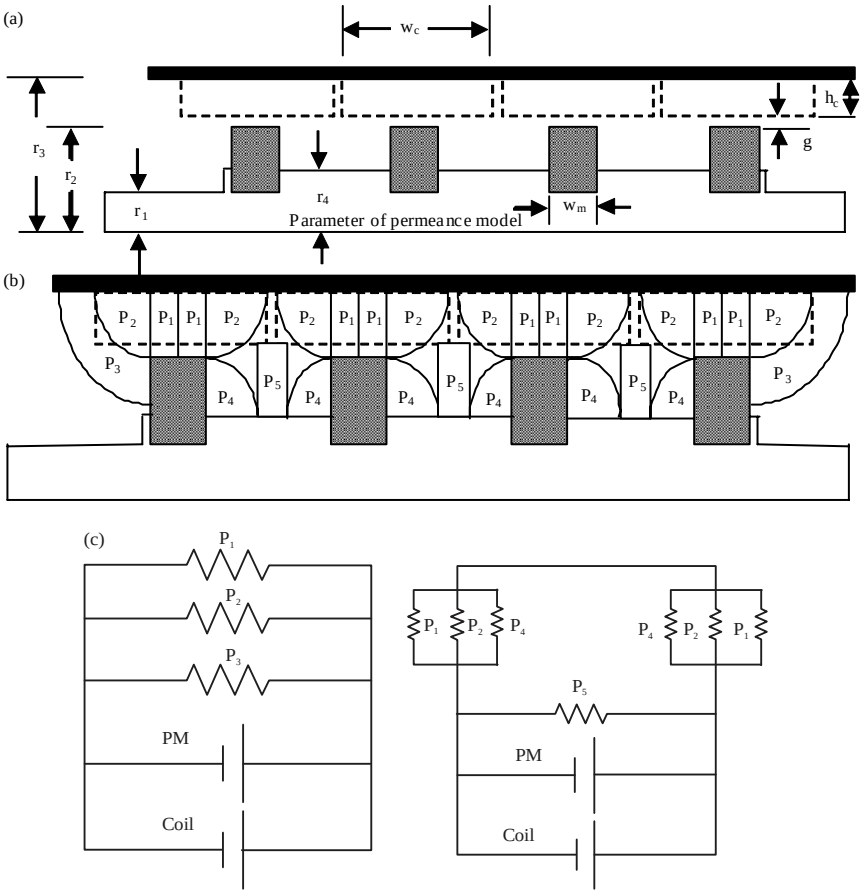

Fig. 6(a-c): Selected PAM model and its magnetic equivalent circuit, (a) Parameter of permeance model, (b) Selected permeance thrust model (c) Magnetic equivalent circuit

$$\Phi_m = B_k A_m \quad (10)$$

where, Φ_m is the magnetic flux at PM, B_k is the magnetic flux density and A_m is the area of the PM. The thrust in each coil can be evaluated by determining the magnetic flux density B_c at the air gap. The magnetic flux density at the air gap can be calculated by determining the magnetic flux density at PM and the coil area. The B_c can be expressed in Eq. 11 as:

$$B_c = \frac{\Phi_m}{A_c} = \frac{\Phi_m}{2\pi\left(r_3 - \frac{h_c}{2}\right)w_c} \quad (11)$$

where, B_c is the magnetic flux density at the air gap, A_c is the area of the coil, r_3 is the inner radius of the back yoke, h_c is the height of the coil and w_c is the width of the coil. According to the permeance model, the magnetic flux density at the air gap B_c is being considered at the end part of the coil and the middle part of the coil.

Thrust produced in the Permeance Analysis Method (PAM) model: After evaluating the magnetic flux density B_c at the end position and middle position, the produced thrust can be calculated using Eq. 12 as follows:

$$F = NIB_c l_c \quad (12)$$

where, F is the produced thrust, I is supplied current, N is the number of turns of the coil, B_c is the magnetic flux density and l_c is the average length of the coil per layer. When the end position is considered to evaluate the thrust, in that case total permeance at the end position $P_{T(end)}$ is determined to evaluate the $B_{c(end)}$. Once obtaining $B_{c(end)}$ the end position thrust, middle position thrust and the total thrust produced by the linear motor can be calculated in Eq. 13-15 as:

$$F_{(end)} = NIB_{c(end)} l_c \quad (13)$$

$$F_{middle} = NIB_{c(middle)} l_c \quad (14)$$

$$F_T = 2F_{end} + 3F_{middle} \quad (15)$$

Calculation of thrust constant (k_f), electrical time constant (T_e) and Mechanical time constant (T_m): The thrust constant k_f depends on the input current and the produced thrust

corresponding to the input current. Once the input current and thrust are established, thrust constant can be calculated using Eq. 16 as:

$$k_f = \frac{F_T}{I} \quad (16)$$

where, F_T is the total thrust of the linear motor and I is the input current of the linear motor. The electrical time constant T_e depends on 2 major parameters of the system such as the total resistance R_T and the total self-inductance L_T. The governing equation for electrical time constant is shown Eq. 17:

$$T_e = \frac{L_T}{R_T} \quad (17)$$

The mechanical time constant is proportional to the mass of the mover m and total resistance R_T and inversely proportional to the square of thrust constant. The governing equation of mechanical time constant is expressed in Eq. 18 as:

$$T_m = \frac{mR_T}{k_f^2} \quad (18)$$

RESULTS AND DISCUSSION

The FEM models were developed for the simulation to predict the size of the linear motor and their corresponding produced thrust. As a requirement for the spray operation, around 60 N thrust is needed to trigger the spray gun. In order to get the best thrust model, firstly single coil and single permanent magnet model was developed and around 0.5 N thrust was produced which was too small to trigger the spray gun. Then 3 coils and 3 permanent magnets model were developed and after the simulation, around 50 N thrust was produced. After obtaining this impressive result, the numbers of coils and magnets were increased one more time and 97 N thrust was obtained. Similar FEM results have been found in (Olaru *et al*., 2012; Kitayama *et al*., 2012; Lee *et al*., 2012). The FEM analysis has been carried out to predict the size of the motor, its displacement and the direction of magnetic flux distribution. Though the analysis method was same as above mentioned research works larger displacement was achieved in this analysis. Because the direction of magnetic flux distribution was redial in this FEM analysis instead of axial flux distribution as used in above mentioned research work. Figure 7 shows the coil and magnet arrangement, magnetic flux flow path and the obtained thrust by using 4 coils and 4 permanent magnets.

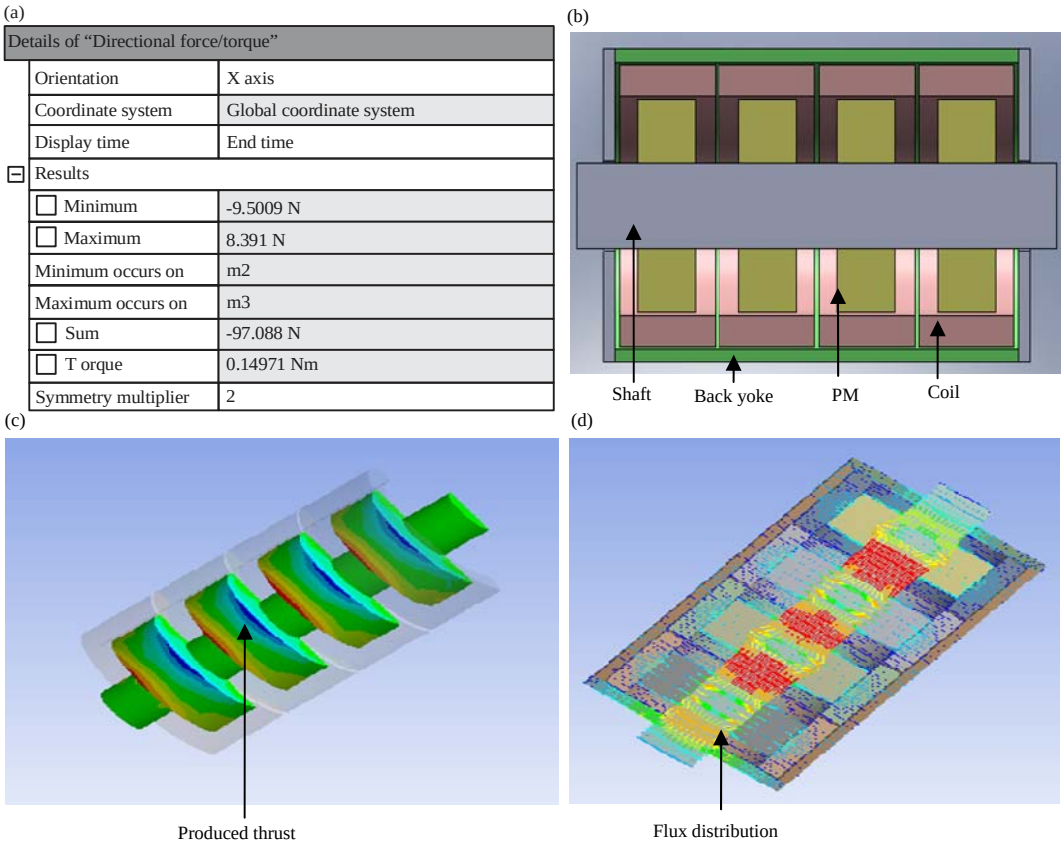

Fig. 7(a-d): Magnetic flux distribution and produced thrust for the arrangement of 4 coils and 4 permanent magnets

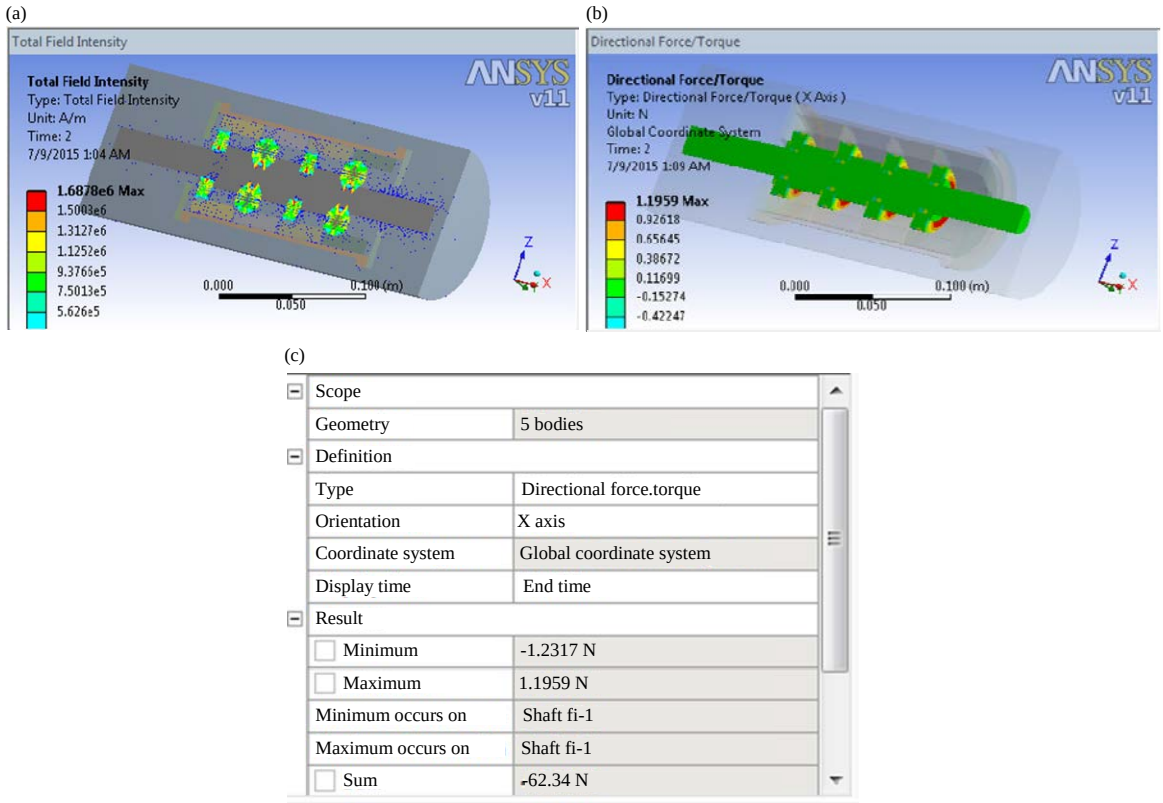

Fig. 8(a-c): Final model and its result, (a) Final model and distributed magnetic flux, (b) Produced thrust and (c) Simulation result

Table 1: Predicted dimensions and materials of the linear motor

Items	Size (mm)	Material	Classification
Back yoke inner radius	35.0	SS400	Ferromagnetic
Back yoke length	156.0		
Coil outer radius	34.5	Copper	Electric conductor
Coil inner radius	24.5		
Permanent magnet outer radius	23.0	NdFeB	Rare earth magnet
Permanent magnet inner radius	10.0		
Shaft diameter	20.0	SS400	Ferromagnetic
Shaft length	266.0		

For triggering, around 60 N thrust is needed and to fulfill the spray operation, 24 mm displacement of the shaft of the linear motor is necessary to open the nozzle. From this point of view the 4 coils and 4 permanent magnets model, which has already been developed was changed in its arrangement of coils and permanent magnets. For the new design the permanent magnets were positioned at the end of each coil. The width of the coil was 35 mm and the thickness was 10 mm while the width of the permanent magnet was 11 mm and thickness was 13 mm. Figure 8 shows the final model with the new arrangement of the coils and permanent magnets, magnetic flux flow and produced thrust. With this arrangement around 62 N thrust was produced which was closer to the required value. In this simulation only 1.75 A current was used as an input current. In this thrust model, the shaft and permanent magnets were used as a mover. No moving yoke was used between the magnets. Therefore, the produced magnetic flux was flown in radial direction. The predicted size and materials of the linear motor are tabulated in Table 1.

Thrust characteristic comparing the result from Finite Element Method (FEM), Permeance Analysis Method (PAM) and experiment: Figure 9 shows the thrust characteristics of the proposed PAM models, FEM model and experimental result. At 1.75 A of input current, the produced thrust obtained from the PAM C FEM simulation and experimental results were 83 N, 97 N and 85 N, respectively. The differences among the results were less than 10% and the experimental results showed that thrust produced linearly to the input current. Due to the linearity characteristic, it can be concluded that adding more current into the linear motor will produce more thrust. At the initial position the linear motor produced 64 N as the input current was 1.75 A. When the mover position was at the middle of the coil, the motor produced 85 N thrust for the same input current. At the end position 43 N was obtained. Since the simulation was carried out at 1.75 A input current, this graphical presentation uses the same input current. At the initial position it produced the minimum thrust and it increased as the displacement changed. The thrust kept increasing until the permanent magnets reached to the mid position of the coils. After that, further changes of the displacement, the thrust was dropped down and at the end of displacement it obtained the minimum value of

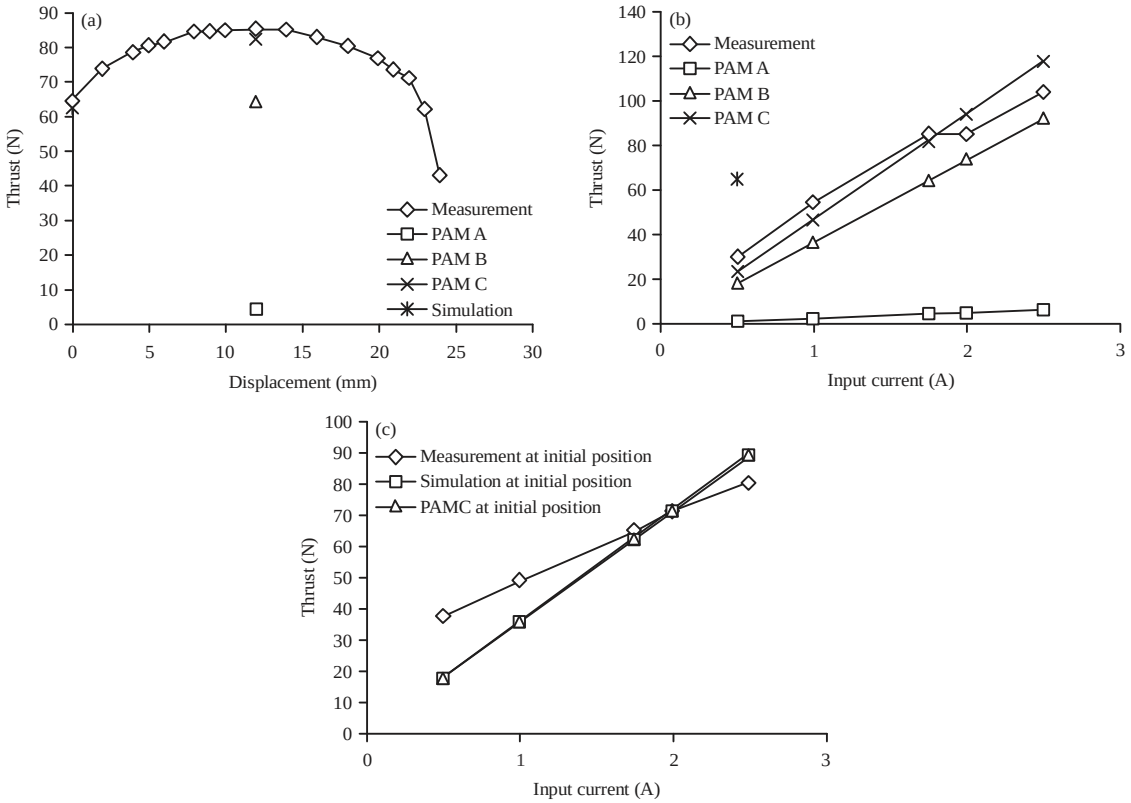

Fig. 9(a-c): Thrust characteristics of the proposed PAM models, FEM model and experimental result, (a) Input current and corresponding thrust, (b) Input current and corresponding thrust at middle position and (c) Input current and corresponding thrust at initial position

thrust again. In this analysis, the difference between the simulation result and experimental result and the PAM C result and the experimental result were 2.7 and 1.83%, respectively. While at the mid position, the difference between the PAM C result and the experimental result was only 3.2%. All the results were quite close to each other and acceptable. Similar results have been found from the studies carried out by (Gieras and Wing, 2002; Zare *et al*., 2011). The obtained data were different among the related research and this analysis because of the difference in topologies and the sizes of the motor. But the linear characteristics what was shown in this analysis is same as the above mentioned research work.

After evaluating the thrust from PAM models A, B and C it was observed that PAM C model was more accurate than the other permeance models therefore, PAM C was used to analyze and evaluate the thrust constant, electrical time constant and the mechanical time constant. The parameter of the back yoke inner radius r_3 was varied from 30-40 mm. The mover length as well as the pitch length l_m was varied from 37-111 mm. The height of the coil h_c was varied from 0-20 mm. This analysis began with fixing the value of back yoke inner radius r_3 and the pitch length l_m. At certain values of r_3 and l_m the coil height h_c was varied and the thrust constant electrical time constant and mechanical time constant were evaluated at every change of coil height.

Effect on constants when the coil height was varied: The effect of thrust constant when the coil height was varied has been analyzed as shown in Fig. 10. The 6 different sizes of the proposed PAM C model had been selected to clarify the variation which were $r_3(30)l_m(37)$, $r_3(30)l_m(111)$, $r_3(35)l_m(74)$, $r_3(35)l_m(111)$, $r_3(40)l_m(37)$ and $r_3(40)l_m(111)$.

Figure 10 shows that when the coil height was increased, the thrust constant also increased but after a certain increment of the height, if the height was further increased, the thrust constant decreased. Therefore, at a certain value of the height of the coil, the maximum thrust constant as well as the optimum value was obtained. The optimum value showed that the saturation of the magnetic material had occurred which was influenced by the magnetic properties. The $r_3(30)l_m(37)$ size achieved the optimum value at 8 mm coil height while $r_3(30)l_m(74)$ and $r_3(30)l_m(111)$ achieved the optimum value at 10 mm. The $r_3(35)l_m(37)$, $r_3(35)l_m(74)$ and $r_3(35)l_m(111)$ obtained the optimum value at 12 mm coil height. Finally $r_3(40)l_m(37)$, $r_3(40)l_m(74)$ and $r_3(40)l_m(111)$ obtained the optimum value at 14 mm coil height. From this analysis it is shown that the size in terms of r_3 and l_m is proportional to the thrust constant. The objective of this analysis was to obtain the optimum size which could meet the requirement.

As Fig. 10 shows, the electrical time constant is proportional to the coil height. For example at $r_3(30)l_m(111)$,

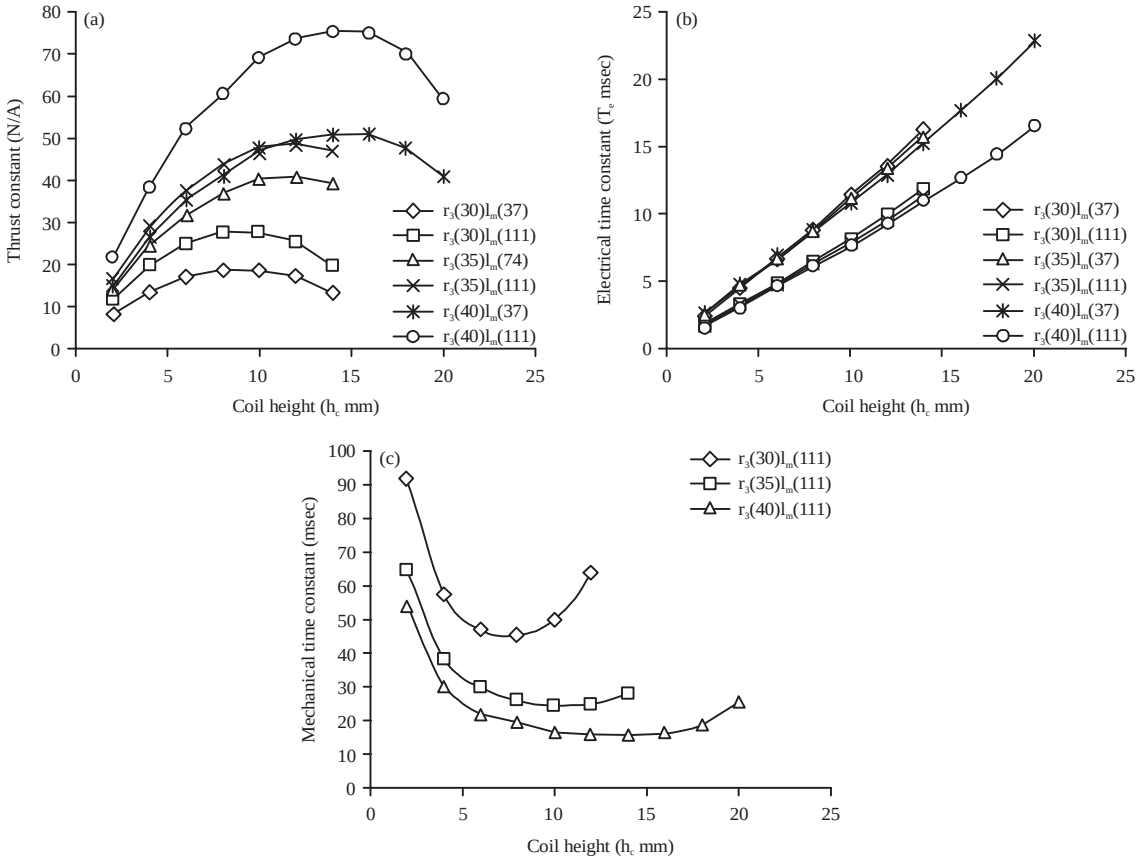

Fig. 10(a-c): (a) Thrust constant, (b) Electrical time constant and (c) Mechanical time constant corresponding to the coil height

the electrical time constant was increased from 1.671-11.84 msec as the coil height varied from 2-14 mm whereas, at $r_3(40)l_m(111)$, the electrical time constant was increased from 1.674-11 msec for the same variation of the coil height. The increment pattern of the electrical time constant was quite identical in both cases. At 14 mm coil height the difference of electrical time constant between $r_3(30)l_m(111)$ and $r_3(40)l_m(111)$ was about 7% which was considered a relatively small percentage.

The effect of the mechanical time constant when the coil height was varied has been analyzed as shown in Fig. 10. Three different sizes, which were $r_3(30)l_m(111)$, $r_3(35)l_m(111)$ and $r_3(40)l_m(111)$ of the PAM C model, had been selected. As Fig. 10 shows, the mechanical time constant decreased as the coil height increased. For example, the mechanical time constant decreased 92-50 msec as the coil height increased from 2-10 mm. At a certain increment of coil height, the minimum mechanical time constant was obtained. From Fig. 10 at $r_3(30)l_m(111)$ of size, the minimum mechanical time constant was 45.6 msec at 8 mm coil height, whereas, at $r_3(35)l_m(111)$ of size, the value of the minimum mechanical time constant of 24.5 msec was obtained at 10 mm coil height, meanwhile at $r_3(40)l_m(111)$ model size, the minimum mechanical time constant was obtained at 12 mm coil height and the value was 15.9 msec. After obtaining the minimum value of the mechanical time constant if the coil height increased the mechanical time constant also increased. As the coil height increases, the mass of the mover gradually decreases, but the total resistance increases and thrust constant increases until its optimum value. After that, the thrust constant decreases. Initially, when the coil height was varied, the increased rate of thrust constant and resistance were quite high. For example, at $r_3(30)l_m(111)$ the increased rates of the thrust constant and resistance were about 48 and 40%, respectively. That is why initially the mechanical time constant decreased rapidly with the variation of coil height. After that, the increased rate of thrust constant and resistance reduced as the coil height was varied. At the minimum value of the mechanical time constant, the increased rates of the thrust constant and total resistance were about 0.3 and 17%, respectively for $r_3(30)l_m(111)$ size of model. Thus the minimum value of the mechanical time constant was achieved. The height of the coil where the minimum mechanical time constant is obtained is the optimum size. At that point, the thrust constant should be the maximum value. The above mentioned analyses have good arguments with previous studies carried by Wang and Howe (2004), Hirata *et al*. (1992) and Mizuno *et al*. (2000). The main objective of this analysis was to optimize the size of the linear motor by comparing the data of the thrust constant, electrical time constant and

Fig. 11(a-c): Fabricated linear motor, mover and coil with coil casing, (a) Fabricated linear motor, (b) Shaft and permanent magnet assembly and (c) Coil and coil casing

Table 2: Optimum parameter of linear motor

Parameters	Values
Back yoke inner radius r_3 (mm)	35.00
Pitch length l_m (mm)	111.00
Coil height h_c (mm)	10.00
Produced thrust F_T (N)	82.52
Thrust constant k_f (N/A)	47.97
Mechanical time constant T_m (msec)	24.50
Electrical time constant T_e (msec)	7.80

mechanical time constant corresponding to coil height. The characteristics curves that obtained in this analysis are similar to the above mentioned research work. But, the lower value of electrical time constant and mechanical time constant obtained in the above mentioned research works compare to this analysis. Because, this analysis was used solid and larger mover compare to the above mentioned research works.

From the above analysis it was seen that at r_3 = 35 mm, the highest thrust was produced at 8 mm coil height and 111 mm pitch length. The value of the highest thrust at this size was 82.93 N. But the highest value of the maximum thrust constant for the same size was obtained at 12 mm coil height. The value of the highest maximum thrust constant was 48.8 N/A. While the minimum mechanical time constant was obtained at 10 mm coil height and the same pitch length and the value of the minimum mechanical time constant was 24.5 msec. The difference of the produced thrust between 8 and 10 mm coil height was 0.49% which can be ignored. On the other hand, the difference of the thrust constant between 10-12 mm coil height was about 1.7% which was also a very small percentage. Therefore, at 10 mm coil height and 111 mm pitch length, which produced almost the highest value of thrust as well as the highest value of the thrust constant with the minimum mechanical time constant can be the optimum size. This size can be considered since it can meet the requirement. Table 2 shows the optimum parameter of the liner motor.

Fabrication of the linear motor: Based on the analysis result, the complete structure of slot-less linear motor has been fabricated as shown in Fig. 11. The mover was composed of 4 pieces of ring-shaped permanent magnets and a shaft. The stator part consists of back yoke and 4 sets of ring shaped coils. A few auxiliary components were required such as linear bush, coil case and 2 units of cover plate. Commercial linear bush cannot be used in this project. Therefore a new design was implemented to complete the task.

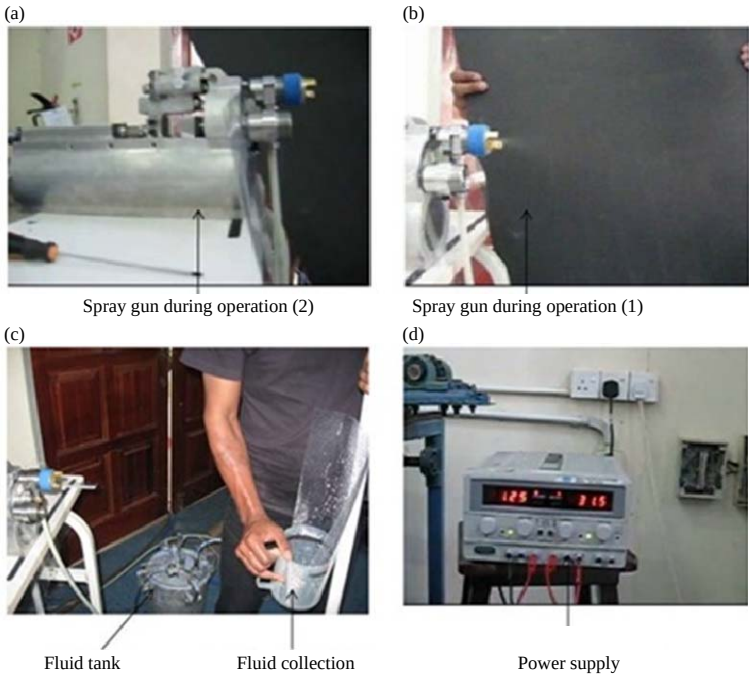

Fig. 12(a-d): Performance test setup of air spray system

Table 3: Comparison of analysis and measurement of k_f, T_e,T_m

Parameter	Calculated (PAM C)	Measurement (prototype)
Thrust constant k_f (N/A)	47.97	49.04
Electrical time constant T_e (msec)	7.8	8.13
Mechanical time constant T_m (msec)	24.5	25.9

PAMC: Permeance analysis method C

Six pieces of segmented magnets were arranged in such a way that they can produce a ring shape. This ring shape magnets were kept inside the motor in an N-S-N-S pattern. The four pieces of ring-shaped magnets were used in this design. All the permanent magnets were in the same dimension. The outer and inner diameters of the magnet were 46 and 20 mm, respectively. The width of the magnet was 11 mm.

The coil casing was designed in such way that it can hold the coil winding properly and provide the minimum gap between the magnet and the coil. Resin material was used to produce the coil casing. Rapid prototyping technology was used to develop the casing which ensures the minimum thickness of the casing. The thickness of the coil casing was only 1 mm. A 156 mm long coil casing provided a 2 mm gap between the coils. There were 4 coils connected in series which were used for this linear motor. A 0.5 mm copper wire was used for winding the coils. The winding process was carried out manually. All the coils used in this research were of the same dimension. Each coil was 35 mm of length, 10 mm of thickness and had at least 715 numbers of turns.

Comparison between the measured value and analysis value of constant parameter: After fabrication, the prototype of the linear motor was tested to measure the thrust constant, electrical time constant and mechanical time constant at the same condition as the analysis was carried out. The electrical time constant is related to the total inductance and the total resistance of the fabricated motor. By using ohmmeter, the total resistance of the motor winding was measured. In order to measure the total inductance, a low voltage AC source was utilized to the motor winding. After getting the actual value of the total resistance and the total inductance of the fabricated motor, the electrical time constant was obtained by using Eq. 17. The mechanical time constant is related to the mass of the mover, the total resistance and the thrust constant of the fabricated motor. After fabricating the mover which consists of shaft and the permanent magnet assembly, the actual mass of the mover was measured using mass measuring scale. Injected current and its corresponding thrust were measured by using the current sensor and the load cell, respectively. From those obtained values of actual current and thrust, actual thrust constant were calculated. After obtaining the total resistance using ohmmeter, the actual mechanical time constant was obtained by using Eq. 18. The measured result was quite identical to the analysis result. Table 3 shows the comparison of constant parameters between the analysis value and the measured value.

Testing performance of the system in air spray: The air spray system was tested using the operating air pressure 8.40 bar and the fluid (water) of 6.5 Bar as recommended for the air spray system. Figure 12 shows the performance test setup of the air spray system.

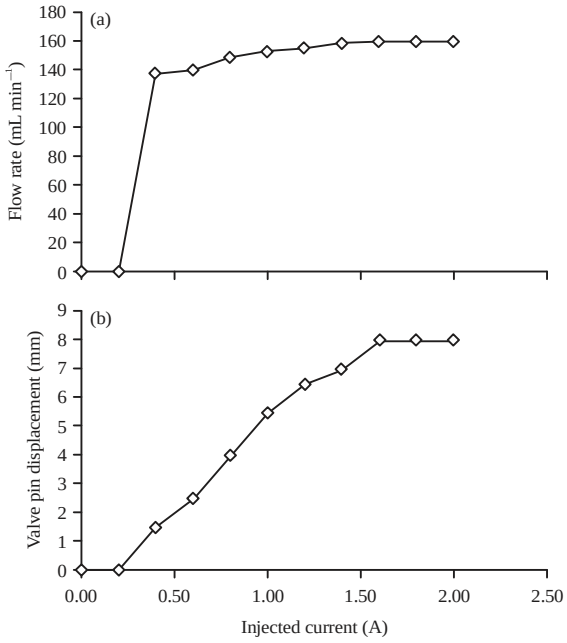

Fig. 13(a-b): Input current and corresponding flow rate and valve displacement of air spray system, (a) Input current and corresponding flow rate of air spray system and (b) Varying position of the pin of the valve with input current

As Fig. 13a shows, when the input current increased, the flow rate also increased and at a certain value of input current, the flow rate reached its maximum value. After that, the flow rate remained constant at the maximum level though the input current was increased. In this system, the nozzle was closed with the help of the needle valve. A mechanical spring was used to hold the valve in its proper position. When the current was injected, the linear motor produced thrust against the spring with the help of the triggering lever and link mechanism and flow starts. At 1.4 A current, the orifice of the nozzle was fully opened and obtained the maximum flow rate of 160 mL min^{-1}. In this system, the current was increased from 0-2 A, but from 1.4-2 A the flow rate remained constant at 160 mL min^{-1}. Figure 13b shows the variation of injected current to the linear motor and the corresponding variation of position of the valve pin. Since the valve was kept in the proper position with the help of the mechanical spring, up to 0.2 A injected current, there was no change in the displacement of the valve pin. This was because the produced thrust corresponding to the 0.2 A current was not enough to open the nozzle orifice. After that, the input current was increased and the valve pin started to move against the spring force. The increment of the displacement of the valve pin was continued as the input current as well as the produced thrust was increased. But after reaching a certain value of input current of 1.4 A, the valve pin displacement stopped to move though the input current was further increased. At 1.4 A input current, the mechanical spring was fully retracted and the orifice of the nozzle was fully opened.

CONCLUSION

The objective of FEM analysis has been achieved. From this analysis, motor size, required thrust, magnetic flux distribution and the materials for stator and mover have been predicted. After that 3 permeance models A, B and C have been developed to optimize the size of the slot-less permanent magnet linear motor. After evaluating the thrust of these models it is observed that PAM C model can generate the required amount of thrust for triggering the spray gun. Therefore, PAM C has been selected to optimized the critical dimension such as coil thickness, pitch length, back yoke inner radius and permanent magnet thickness etc. The effects of thrust constant, electrical time constant and mechanical time constant have been analyzed to optimize the dimensions of the motor. Finally using these optimized data the motor has been fabricated and tested. The analysis results and the experimental results are quite identical.

ACKNOWLEDGMENTS

The authors acknowledge all the supporting members in electrical machine and power laboratory of faculty of engineering, Universiti Putra Malaysia (UPM) to complete the research and the management of Universiti Tenaga Nasioal (UNITEN) for their permission to conduct the research at UPM. The authors also acknowledge the Malaysian Education Ministry for providing the fund for this project in Fundamental Research Grant Scheme (FRGS).

REFERENCES

Al-Sharif, L., S. Taifour and M. Kilani, 2010. Simulation and verification of the axial force of a linear permanent magnet synchronous actuator. Int. J. Applied Electromagn. Mech., 32: 249-265.

Aris, I.B. and A.K.M. Parvez Iqbal, 2006. Design and fabrication of a Cartesian painter robot for the construction industry. Int. J. Mech. Eng. Educ., 34: 125-144.

Cawthorne, W.R., P. Famouri, J. Chen, N.N. Clark and T.I. McDaniel *et al*., 1999. Development of a linear alternator-engine for hybrid electric vehicle applications. IEEE Trans. Veh. Technol., 48: 1797-1802.

Chen, Y.M., S.Y. Fan and W.S. Lu, 2008. Performance analysis of linear permanent-magnet motors with finite-element analysis. IEEE Trans. Magn., 44: 377-385.

Clark, R.E., D.S. Smith, P.H. Mellor and D. Howe, 1995. Design optimisation of moving-magnet actuators for reciprocating electro-mechanical systems. IEEE Trans. Magn., 31: 3746-3748.

Eastham, J.F., 1990. Novel synchronous machines: Linear and disc. IEE Proc. B (Electr. Power Applic.), 137: 49-58.

Fujiwara, R., T. Shinshi and M. Uehara, 2013. Positioning characteristics of a MEMS linear motor utilizing a thin film permanent magnet and DLC coating. Int. J. Autom. Technol., 7: 148-155.

Gieras, J.F. and M. Wing, 2002. Permanent Magnet Material and Circuits. In: Permanent Magnet Motor Technology: Design and Applications, Gieras, J.F. and M. Wing (Eds.). 2nd Edn., Marcel Dekker Inc., New York, USA., ISBN-13: 9780824743949, pp: 43-86.

Hirata, K., Y. Kagami, M. Yanosaka, Y. Ishihara and T. Todaka, 1992. Thrust calculation of linear pulse motors using a combined technique employing the finite element method and the permeance analysis method. IEEE Trans. Magn., 28: 1394-1397.

Kitayama, F., K. Hirata and Y. Asai, 2012. Performance evaluation of linear oscillatory actuator for active control engine mount. IEEJ Trans. Ind. Applic., 132: 1091-1096.

Lee, J., E.M. Dede, D. Banerjee and H. Iizuka, 2012. Magnetic force enhancement in a linear actuator by air-gap magnetic field distribution optimization and design. Finite Elem. Anal. Des., 58: 44-52.

Liu, X., K. Wu, Y. Ye and K. Lu, 2012. Design and optimization of the new H-module linear actuator. IEEE Trans. Magn., 48: 4188-4191.

Low, K.S., Y.Z. Deng, M.T. Keck and C.W. Koh, 1998. A high performance linear motor drive for integrated circuit's leads inspection system. Proceedings of the 24th Annual Conference of the IEEE Industrial Electronics Society, Volume 3, August 31-September 4, 1998, Aachen, Germany, pp: 1321-1325.

Masada, E., 1995. Linear drives for industrial applications in Japan-history existing state and future prospect. Proceedings of the 1st International Symposium on Linear Drives for Industry Applications, May 31-June 2, 1995, Ioujima, Nagasaki, Japan, pp: 9-12.

Mizuno, T., M. Iwadare, M. Nanahara, K. Koyama, T. Anzai, M. Nirei and H. Yamada, 2000. Considerations on electrical and mechanical time constants of a moving-magnet-type linear DC motor. Sens. Actuat. A: Phys., 81: 301-304.

Olaru, R., C. Astratini-Enache and C. Petrescu, 2012. Analysis and design of a moving-magnet type linear actuator with repulsive magnetic force. Int. J. Applied Electromagn. Mech., 38: 127-137.

Park, K., E.P. Hong and K.H. Lee, 2001. Development of a linear motor for compressors of household refrigerator. Proceedings of the 3rd International Symposium on Linear Drives for Industry Applications, October 17-19, 2001, Nagano, Japan, pp: 283-286.

Parvez Iqbal, A.K.M., I. Aris, N. Misron, M.H. Marhaban and W. Asrar, 2011a. Design process involved in developing mechanism of linear motor operated multiple spray operations spray gun. Austr. J. Basic Applied Sci., 5: 843-850.

Parvez Iqbal, A.K.M., I. Aris, N. Misron, M.H. Marhaban and W. Asrar, 2011b. Thrust analysis and measurement of a tubular linear permanent magnet motor in spray application. J. Japan Soc. Applied Electromagn. Mech., 19: S83-S86.

Shi, Y. and S. Chang, 2013. Modeling and experiment of electromagnetic linear actuator for fuel injector of engine. Trans. Chin. Soc. Agric. Mach., 44: 21-26.

Utsuno, M., M. Takai, T. Yaegashi, T. Mizuno, H. Yamamoto, K. Shibuya and H. Yamada, 2001. Efficiency characteristics of a linear oscillatory actuator under simulated compressor load. Proceedings of the 3rd International Symposium on Linear Drives for Industry Applications, October 17-19, 2001, Nagano, Japan, pp: 264-267.

Wang, J. and D. Howe, 2004. Design optimization of radially magnetized, iron-cored, tubular permanent-magnet machines and drive systems. IEEE Trans. Magn., 40: 3262-3277.

Watada, M., K. Yanashima, Y. Oishi, D. Ebihara and H. Dohmeki, 1993. Improvement on characteristics of linear oscillatory actuator for artificial hearts. IEEE Trans. Magn., 29: 3361-3363.

White, M.A., K. Colenbrander, R.W. Olan and L.B. Penswick, 1996. Generators that won't wear out. Mech. Eng., 118: 92-96.

Zare, M.R., M. Norhisam, M. Mariun, I. Aris, H. Wakiwaka and M. Nirei, 2011. High thrust density transverse flux linear motor: Thrust analysis and driving method. Int. Rev. Electr. Eng., 6: 2229-2236.

Zhu, Y.W., S.G. Lee and Y.H. Cho, 2011. Thrust and normal force characteristics analysis of linear synchronous motor for direct drive conveyer. Int. J. Applied Electromagn. Mech., 36: 41-48.